Coercivity Enhancement of Hexagonal Ferrites

Silvia E. Jacobo[1,a] and Paula G. Bercoff [2,b]

[1]Laboratorio de Fisicoquímica de Materiales Cerámicos Electrónicos (LAFMACEL). Facultad de Ingeniería (UBA) – INTECIN. Paseo Colón 850, (1063) Ciudad Autónoma de Buenos Aires, Argentina

[2]Facultad de Matemática, Astronomía y Física, Universidad Nacional de Córdoba. Instituto de Física Enrique Gaviola, CONICET. M. Allende s/n, Ciudad Universitaria. 5000 Córdoba, Argentina

[a]sjacobo@fi.uba.ar, [b]bercoff@famaf.unc.edu.ar (corresponding author)

Abstract. Hexagonal ferrites have been widely used as permanent magnets since their discovery in the 1950s. In spite of their relatively modest magnetic properties, ferrite magnets still show the best performance-to-cost ratio and different investigators are trying to improve their magnetic capabilities by using different synthesis methods and compositions. Different scientific investigations and techniques (Mössbauer spectrometry, X-ray diffraction, and magnetic measurements) have allowed to optimize the permanent magnet properties of rare earth substituted hexagonal ferrite magnets such as La-Co and Nd-Co Sr and Ba ferrites. However, the solubility of rare earth ions in M-type hexaferrite is very low and their introduction leads to the formation of secondary phases, which must be avoided in order to obtain permanent magnets with optimal properties.

We report results on enhanced coercivity of hexagonal Sr ferrites with Nd-Co substitution synthesized by the self-combustion method and calcination at 1100°C for two hours. The synthesis of this kind of ferrite is performed with a deficient, non-stoichiometric iron content (ratio Fe/ $Sr_{1-x}R_x$ of 10 and 11 instead of 12) in order to explore the presence of secondary phases. Comparison with samples of the same composition and stoichiometric formulation is made. Samples with lower iron content show the highest saturation magnetization, remanence and/or coercivity, indicating that the best results for applications of this ferrite will be obtained with an iron deficiency in the stoichiometric formulation. Nd substitution enhances the ferrite anisotropy and coercivity with respect to the unsubstituted sample.

1. Introduction

Ever since their discovery by Philips between 1952 and 1956, M-type ferrites have increasingly become widely used for applications such as permanent magnets, plasto-ferrites, injection moulded pieces, microwave devices and magnetic recording media [1-4] mainly because of their high coercivities and relatively low production costs.

Wet routes such as sol-gel and self-combustion methods have been successful in producing homogeneous nanosized ferrite crystallites at much lower calcination temperatures than other methods [5, 6]. It is widely accepted that calcination temperature is closely related to grain size, secondary phases, site occupancy, magnetocrystalline anisotropy and coercivity. Therefore, controlling this parameter of the synthesis procedure may lead to optimization of the products properties. While low temperatures may prevent grain growth and keep high coercivities, a fully crystalline structure with optimal sites' occupancy may not be possible to achieve. Also, the appearance of secondary phases must be prevented. Since different iron compounds are reported to be the main secondary phases in hexaferrites, different authors proposed iron-deficient formulations. In particular, Fu *et al*. prepared non-stoichiometric Sr hexaferrite with a Fe/Sr ratio of 10.8 and no substitution [7]. These authors observed that as the calcination temperature is increased from

650 °C to 900 °C an increase in coercivity is observed, but when the temperature is further increased beyond 900 °C, a decrease in coercivity is noticed. They explain the increase in coercivity at lower temperatures as a result of the development of the M phase as temperature increases up to 900 °C. The decrease in coercivity for temperatures above 900 °C is attributed to the increase in particle size.

It has been reported by different authors that both saturation magnetization as well as magnetocrystalline anisotropy of M-type ferrite fine particles can be modified by the substitution of rare earths [8-10]. However, the solubility of rare-earth ions in Sr-hexaferrites is very low and their addition leads to the formation of secondary phases, which must be controlled in order to obtain permanent magnets with optimal properties [9-12]. J. F. Wang *et al*. have investigated Sm-doped Sr hexaferrite particles hydrotermally synthesized [13]. They reported that the intrinsic coercivities of Sm-doped Sr hexaferrite improved when compared with non-substituted strontium hexaferrite.
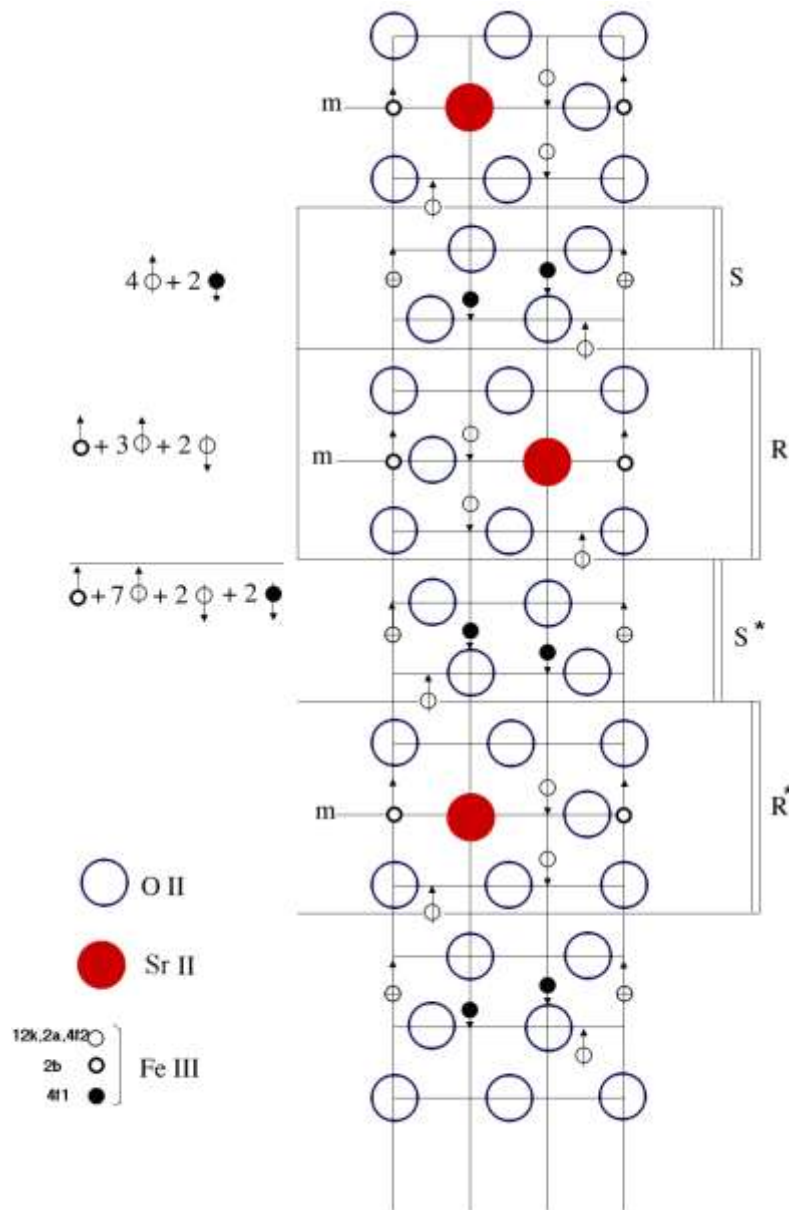
Fig. 1. General structure of M-type hexaferrite with R and S blocks. Crystalline sites of iron, strontium and oxygen are indicated with different symbols (* indicates a 180° rotation).

The general structure of M-type hexaferrite ($AO \cdot 6Fe_2O_3$ or $AFe_{12}O_{19}$, where A is a divalent ion such as Ba^{2+}, Sr^{2+}, Pb^{2+}, etc.) is hexagonal with space group *P63/mmc*. The crystalline structure is constructed from two building blocks, namely S and R, as shown in Figure 1 [14]. The oxygen atoms are close-packed with the A and Fe ions in the interstitial sites. There are ten layers of oxygen atoms along the *c* axis and the iron atoms are positioned at five crystallographically different sites. The S (Fe_6O_8) blocks are spinels with two oxygen layers and six Fe^{3+} ions. As for the hexagonal R (AFe_6O_{11}) blocks, they consist of three oxygen layers with one of the oxygen anions replaced with an A ion (A = Sr in Figure 1). In this kind of hexaferrites, the iron ions occur on five different sites: the octahedral sites, crystallographically known as 2a, 12k, and 4f2, one tetrahedral site 4f1 and one trigonal bypyramidal site, 2b. In the magnetically ordered state of $SrFe_{12}O_{19}$, the 12k, 2a, and 2b sites have their spins aligned parallel to each other and to the crystallographic *c* axis, whereas those of 4f2 and 4f1 point in the opposite direction.

In this work, we present the results obtained on the structural and magnetic properties of non-stoichiometric strontium hexaferrite samples prepared by the self-combustion method. An iron deficient formulation is proposed to prevent the appearance of segregated phases. In order to improve coercivity, Nd and Co ions were introduced as substitutions in the hexagonal lattice.

We studied systems with different Fe/Sr ratios in an attempt to determine the optimal relationship so as to obtain single-phase materials while keeping the crystalline structure unchanged and improve the magnetic properties.

2. Experimental Technique

Samples of composition $SrFe_xO_{19}$ (for $x = 12$, 11 and 10, being $x=12$ the stoichiometric value for phase M) and substituted samples $Sr_{0.7}Nd_{0.3}Fe_{12-y}Co_{0.3}O_{19}$ (for $y = 0.3$, 1.3 and 2.3) were prepared by the self-combustion method. The chemical precursors used for these experiments were $Fe(NO_3)_3 \cdot 9H_2O$, $SrCO_3$, Nd_2O_3, $Co(CH_3COO)_2 \cdot 4 H_2O$, as it was earlier reported [15, 16]. The ratio citric:nitric acid was fixed in 2:1 for each experiment. Aqueous suspensions were stirred and heated for several hours until the sol turned into a dried gel. Then the dried gel was ignited in a corner and a combustion wave spontaneously propagated through the whole gel converting it into loose magnetic powder. Powders were heat-treated in air at 1100ºC for two hours. The non-stoichiometric compositions and sample labels for the powders heated at 1100ºC are given in Table 1. The oxygen content was calculated assuming the following valences: Sr^{2+}, Nd^{3+}, Co^{2+} and Fe^{3+}.

**Table 1.** Labels and nominal composition of the studied samples

Sample label	Nominal Composition
F12N0	$SrFe_{12}O_{19}$
F11N0	$SrFe_{11}O_{17.5}$
F10N0	$SrFe_{10}O_{16}$
F12N3	$Sr_{0.7}Nd_{0.3}Fe_{11.7}Co_{0.3}O_{19}$
F11N3	$Sr_{0.7}Nd_{0.3}Fe_{10.7}Co_{0.3}O_{17.5}$
F10N3	$Sr_{0.7}Nd_{0.3}Fe_{9.7}Co_{0.3}O_{16}$

The structural analysis of the powders was done by X-ray diffraction (XRD) using a Philips diffractometer and CuKα radiation. The patterns were taken between $2\theta = 20º$ and 70º with a step of 0.02º. A FE-SEM Sigma Zeiss microscope with an Oxford EDS spectrometer was used for image and chemical characterization. A vibrating sample magnetometer Lakeshore 7300 was used to measure the magnetic properties at room temperature. Hysteresis loops *M vs H* were measured with a maximum applied field of 15 kOe. Since the loops did not saturate at 15 kOe, the value of saturation magnetization M_S for each sample was calculated by extrapolating *M vs 1/H* to 0. Fe

Mössbauer spectroscopy was performed at room temperature, in transmission geometry. A [57]Co(Rh) source was used with a constant acceleration drive. The spectrometer was calibrated using an α-Fe foil. Mössbauer spectra were fitted with the NORMOS (SITE) program [17]. Isomer shift values are reported relative to α-Fe whereas the velocity abscissas of the spectra are relative to the source.

3. Structural Characterization

3.1 X-ray Diffraction. Figure 2 shows X- ray diffraction patterns of unsubstituted (left panel) and substituted samples (right panel). X-ray analysis reveals that, in all patterns, the main peaks correspond to the hexagonal M phase (ICSD 202518). Samples F11N0, F10N0 and F10N3 are single-phase, while F12N0 contains 8% hematite. Some secondary phases such as hematite (~7%, ICSD 66756), Nd ferrate $NdFeO_3$ (~4%, ICSD 153441) and Co_2FeO_4 (~5%, ICSD 98553) are found in F12N3 and F11N3, according to Rietveld refinement of the corresponding spectra (not shown here, previously published in [18]).
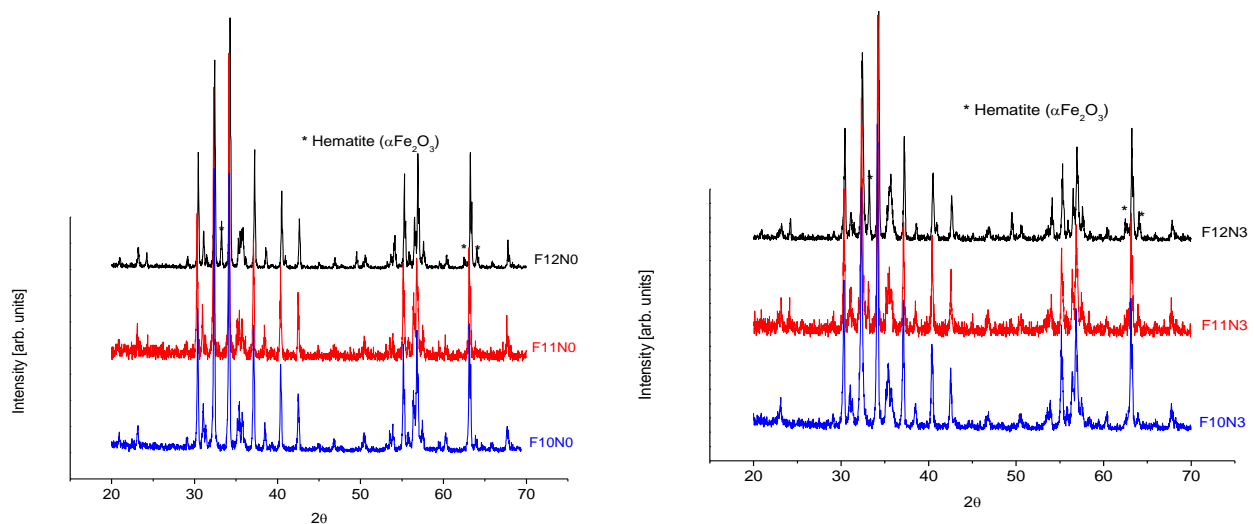
**Fig. 2.** X ray diffraction patterns of unsubstituted (left panel) and substituted samples (right panel).

Table 2 shows that crystallite sizes D as well as cell parameters $a=b$ and c are modified with substitution, x. In every case, D is reduced. It is noticeable that crystallite size is smaller in those samples where secondary phases are present. This phenomenon is related to the presence of foreign phases that inhibit crystalline growth. Similar results were reported by Rezlescu *et al*. [19]. The parameters a and c are slightly modified with substitution as the ionic radii of Nd^{3+} and Co^{2+} are very close to the radius of the replaced ions Fe^{3+} and Sr^{2+}. The slight increase of the cell volumes V_{cell} for F10N0 and F10N3 can be related to the absence of secondary phases.

**Table 2.** Crystallite size D, cell parameters a and c, and unit cell volumes V_{cell}.

Sample	D [±1 nm]	a [±0.0001 Å]	c [±0.0001 Å]	V_{cell} [±1 Å³]	Secondary phases
F12N0	70	5.8718	23.0024	686	Yes
F12N3	55	5.8752	22.9760	686	Yes
F11N0	122	5.8798	23.0321	689	No
F11N3	87	5.8767	23.0040	688	Yes
F10N0	110	5.8858	23.0416	691	No
F10N3	110	5.8976	23.0440	693	No

3.2 Microscopy and Elemental Analysis. Scanning Electron Microscopy (SEM) images of the samples with Nd-Co substitution are shown in Figure 3. All the particles are hexagonal platelets. Samples F12N3 and F11N3, which contain few amounts of secondary phases, are composed of particles of the order of 100 nm. Sample F10N3, which is single-phase, is formed by much lager particles. The effect of particle growth in single phase materials and growth constraint in multi-phase systems has also been reported by other authors [20]. The difference between crystallite sizes *D* and particle sizes indicates that the particles are polycrystalline.

X-ray maps show that the cationic distribution within the particles is very homogeneous for all the studied samples. The results are very similar and are shown in Figure 4 for sample F11N3. EDS analyses confirm the nominal composition in every case.


F12N3   F11N3   F10N3
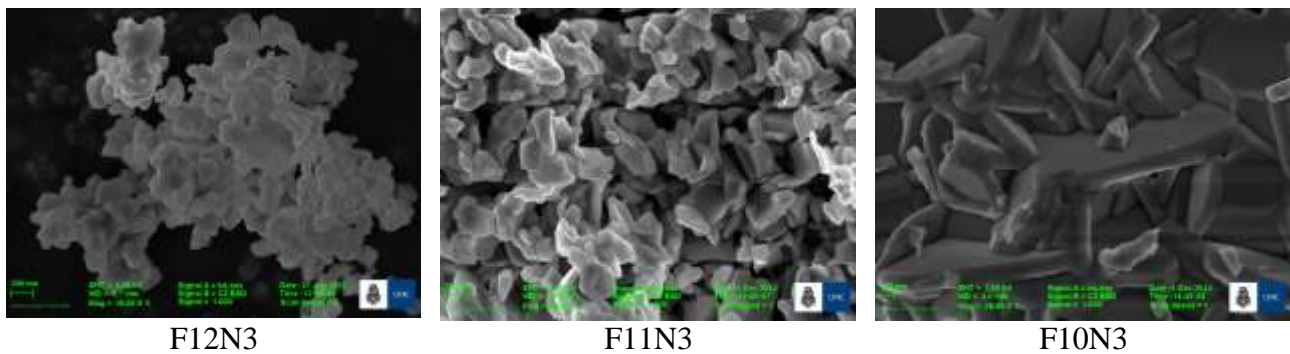
Fig. 3. SEM images of the substituted samples. The bar corresponds to 200nm.
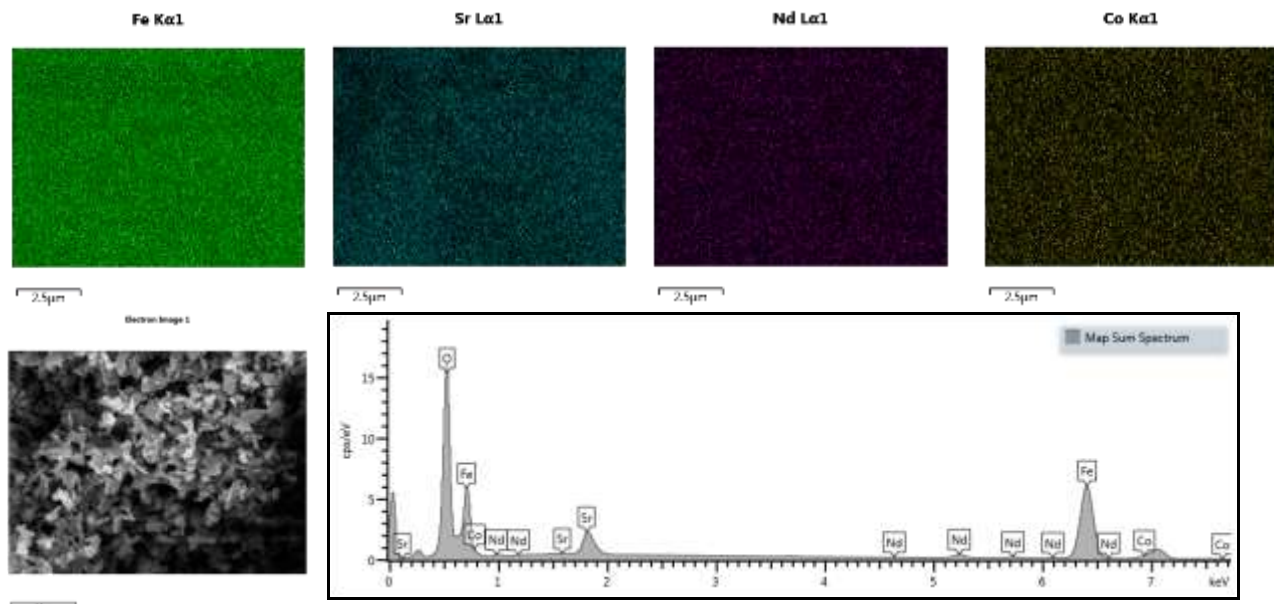
Fig. 4. X-ray maps (from left to right: Fe Kα1, Sr Lα1, Nd Lα1 and Co Kα1) of sample F11N3. The corresponding secondary electron image, as well as the map sum spectrum, are also Shown.

3.3 Mössbauer spectrometry. Room temperature Mössbauer spectra of all the studied samples were analyzed in terms of five Zeeman sextets, except for samples F12N0, F12N3 and F11N3, where another contribution from some hematite was included. The intensity of each sextet is directly proportional to the number of iron atoms in each site, thus giving an estimate of the occupancy percentage in the corresponding site. Mössbauer spectrum of sample F11N0 ($SrFe_{11}O_{19}$) is shown in Figure 5.
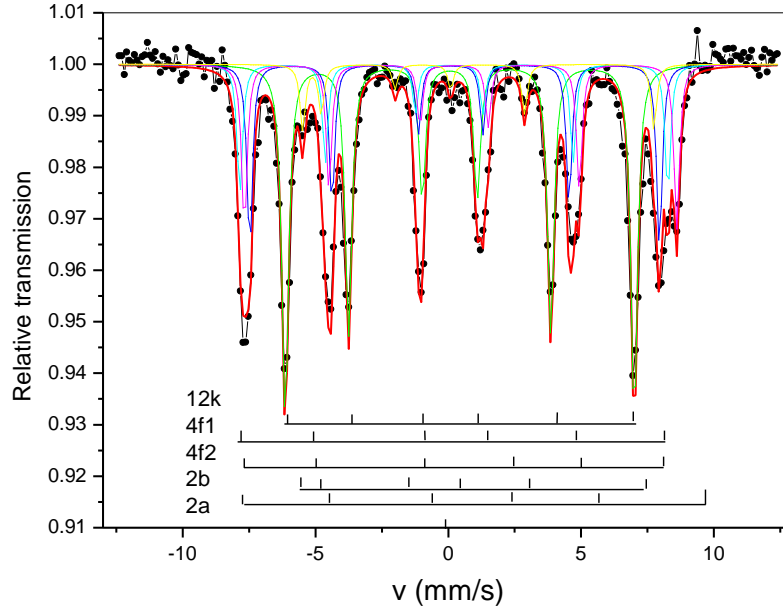
Fig. 5. Room-temperature Mössbauer spectrum of sample F11N0. Dots indicate measured points and solid lines correspond to the fit. Crystalline sites are indicated below the spectrum.

Tables 3a and 3b show the hyperfine parameters of the studied samples. All the substituted samples have higher hyperfine field H_f values. This result is related to certain perturbation in the superexchange interaction when Co^{2+} enters the 4f2 and the 2a sites. The isomer shifts *IS* follow the sequence 4f2>12k>2b>4f1≥2a. On 4f2 sites *IS* decreases with Fe defect. This may be attributed to a decrease in the Fe-O distance for 4f2 sites due to vacancies in 2b sites. This behavior is accompanied with an increase of the quadrupole splitting (*QS*). These results are related to the hexaferrite structure [21]. Hyperfine parameters of sites 4f1 and 2b do not significantly change with Fe defect or with cation substitution.

Table 3a. Isomer shift *IS*, quadruple splitting *QS* and hyperfine field H_f for octahedral sites 12k, 2a and 4f2.

	12k			2a			4f2		
	IS [mm s^{-1}]	*QS* [mm s^{-1}]	H_f [T]	*IS* [mm s^{-1}]	*QS* [mm s^{-1}]	H_f [T]	*IS* [mm s^{-1}]	*QS* [mm s^{-1}]	H_f [T]
F12N0	0.35	0.39	41.0	0.24	0.07	51.3	0.50	0.07	51.3
F12N3	0.35	0.39	41.6	0.21	0.05	51.5	0.45	0.05	51.3
F11N0	0.35	0.41	41.5	0.22	0.22	51.3	0.40	0.22	51.6
F11N3	0.35	0.39	41.7	0.19	0.11	51.5	0.44	0.11	51.4
F10N0	0.35	0.39	40.6	0.21	0.22	50.1	0.38	0.22	50.8
F10N3	0.35	0.39	42.0	0.23	0.22	51.1	0.41	0.22	51.6

Table 3b. Isomer shift *IS*, quadruple splitting *QS* and hyperfine field H_f for tetrahedral sites 4f1 and 2b.

	4f1			**2b**		
	IS [mm s^{-1}]	*QS* [mm s^{-1}]	H_f [T]	*IS* [mm s^{-1}]	*QS* [mm s^{-1}]	H_f [T]
F12N0	0.27	0.19	48.7	0.27	2.21	40.9
F12N3	0.25	0.17	48.9	0.27	2.21	40.9
F11N0	0.26	0.17	49.0	0.26	2.25	41.3
F11N3	0.25	0.17	48.9	0.27	2.18	41.1
F10N0	0.26	0.15	48.3	0.25	2.22	40.5
F10N3	0.27	0.13	49.1	0.25	2.21	41.5

Figure 6 shows site occupancy in the five crystallographic sites, obtained from Mössbauer results for all samples with different iron content (non-substituted samples are indicated with solid symbols and substituted samples with open symbols). Iron vacancies are not proportionally distributed in all sites.
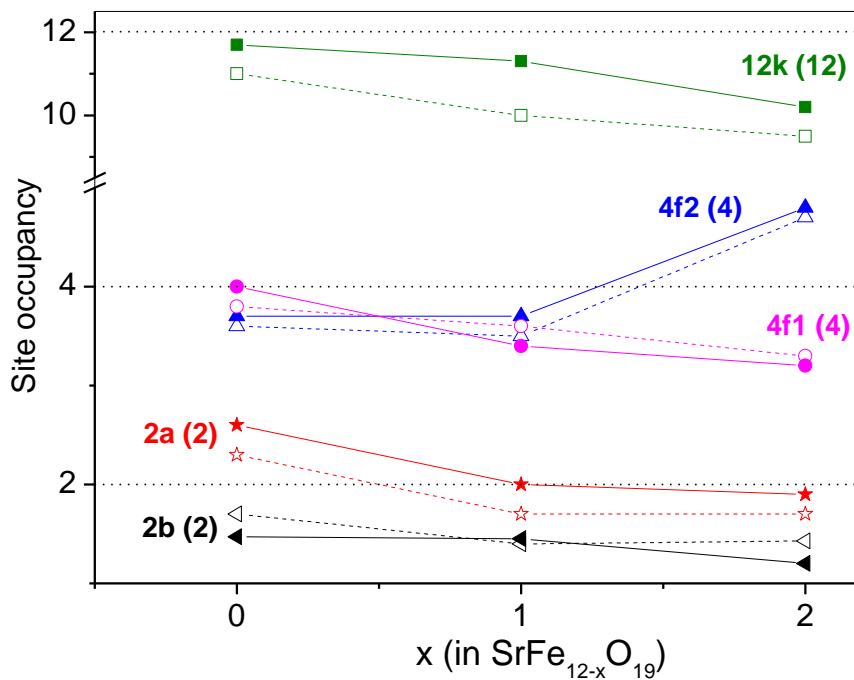
Fig. 6. Fe^{3+} occupancy of the five sites in the M-type hexagonal structure for samples with different iron content (Table 1). Unsubstituted samples are indicated with solid symbols and solid lines and Nd-Co substituted samples are represented with open symbols and dashed lines. The numbers between parenthesis indicate the theoretical value of occupation for the corresponding site.

For a fixed composition (*x*), Fe content diminishes with substitution in the octahedral sites 12k and 2a and in the tethraedral site 4f2. For a very low Fe content (*x*=2) site occupancy shows a different behavior for 4f2, which increases above the theoretical value. These results may explain the anomalous tendency in cell volumes and in saturation magnetization.

3.4 Magnetic Characterization. Hysteresis loops of samples with and without substitution are shown in Figures 7a to 7c. In every case, Nd-Co substitution improves both remanence and coercivity. Saturation magnetization is reduced with substitution, but this effect is not strong

enough to reduce the M_r/M_S ratio. In fact, M_r/M_S is enhanced (see Table 4). The sample with optimal properties for uses in permanent magnets is F11N3, despite having a total of 16% secondary phases. Tiene muy Buena ocupación de los sitios 12k y 2b, comparable a la estequiométrica. In Figure 7d the *M vs H* curves of all the substituted samples are shown for comparison. Saturation magnetization M_S, remanence M_r and coercivity H_C are higher for sample F11N3 (see also Table 4).

The increase in coercivity can be related to the magnetocrystalline anisotropy increase with Nd-Co substitution while the lower magnetization values can be related to secondary non-magnetic phases. The presence of secondary phases does not appreciably modifies coercivity (see results for samples with *x*=12 and *x*=10). Therefore, the Fe^{3+} ions in different sites make different contributions to the magnetic properties of the strontium ferrite. It has also been proved that the single-ion anisotropy of the iron ions in 4f2 and 2b sites is the main origin of the uniaxial magnetocrystalline anisotropy of Sr-ferrite [22].

As discussed above, Nd-Co ions prefer to occupy the 4f2 and 2a crystallographic sites. When Fe^{3+} ions are substituted by Nd-Co ions, the Fe^{3+}–O–Fe^{3+} superexchange becomes weak, causing degradation in saturation magnetization.

(a)   **(b)**

(c)   **(d)**
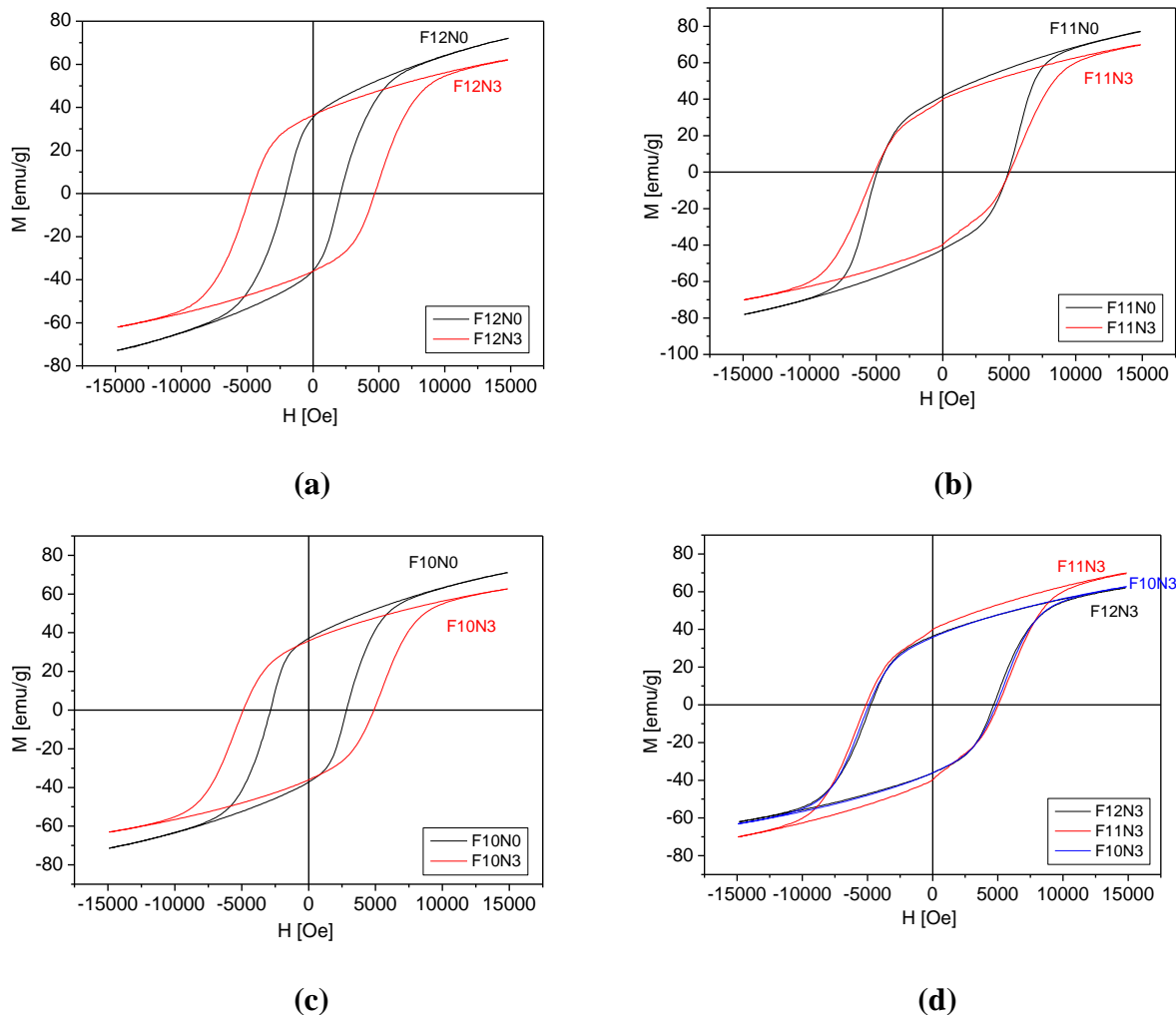
Fig. 7 (a-c). Hysteresis loops for all the studied samples, and **(d)** comparison between the substituted samples.

Table 4. Maximum magnetization at 15 kOe $M_{\text{max-15kOe}}$, saturation magnetization M_s, remanence M_r, M_r/M_s ratio, coercivity H_c and maxima of susceptibility χH_{C1} and χH_{C2}

Sample	$M_{\text{max-15kOe}}$ [±0.5 emu/g]	M_s [±0.5 emu/g]	M_r [±0.5 emu/g]	M_r/M_s	H_C [±5 Oe]	χH_{C1} [±20 Oe]	χH_{C2} [±20 Oe]
F12N0	72.5	91	35.3	0.39	2060	1810	3430
F12N3	61.9	75	35.4	0.47	4725	4870	5410
F11N0	77.4	97	41.6	0.43	4930	4070	5800
F11N3	69.7	87	40.0	0.46	5120	5300	7190
F10N0	70.9	88	37.0	0.42	2840	2535	3620
F10N3	63.7	78	35.8	0.46	4885	5093	6160

Magnetic susceptibility $\chi = dM/dH$ is related to the inversion-field distribution in magnetic systems, therefore it is often calculated to evaluate the existing magnetic interactions. The maximum in dM/dH (denoted χH_C) is the same as coercivity H_C in systems with a single magnetic phase and a unimodal inversion-field distribution.

Susceptibility χ, for all the studied samples, was calculated as the derivative of the upper branch of the hysteresis loop M with respect to H and is shown in Figure 8. The fitting of these curves was performed using Voigt functions and the program PeakFit 4.12. The position of the peaks was determined with an error of about ±20 Oe, since displacements of this amount did not appreciably alter the regression coefficient (probably because of the experimental values' dispersion). In every case, two magnetic contributions were needed to fit χ *vs H*.

Since most of the samples are single-phase and neither of the secondary phases in F12N3 and F11N3 are likely to contribute appreciably to dM/dH (for a more detailed analysis on this, refer to [18]) the two contributions to susceptibility are assigned to an inhomogeneous cationic distribution and/or a lattice distortion related to the increase in magnetocrystalline anisotropy. These contributions give rise to two magnetic orderings: one with lower χH_C ($\chi H_C 1$ in Table 4) and another with higher anisotropy regions and therefore higher χH_C ($\chi H_C 2$ in Table 4). Because of the interaction between these magnetic arrangements, H_C results in an intermediate value of coercivity (H_C in Table 4).

This effect has already been reported on similar samples in a previous paper [15], where the two observed contributions to χ converged into one after sintering, indicating that the harder magnetic phase was originated in an inhomogeneous cationic distribution. In the present case; however, longer calcination times do not anneal out this effect, probably because of the higher occupancy of the crystalline sites due to the higher Fe/Sr ratios selected for this work, which might slow down cation thermal migration.
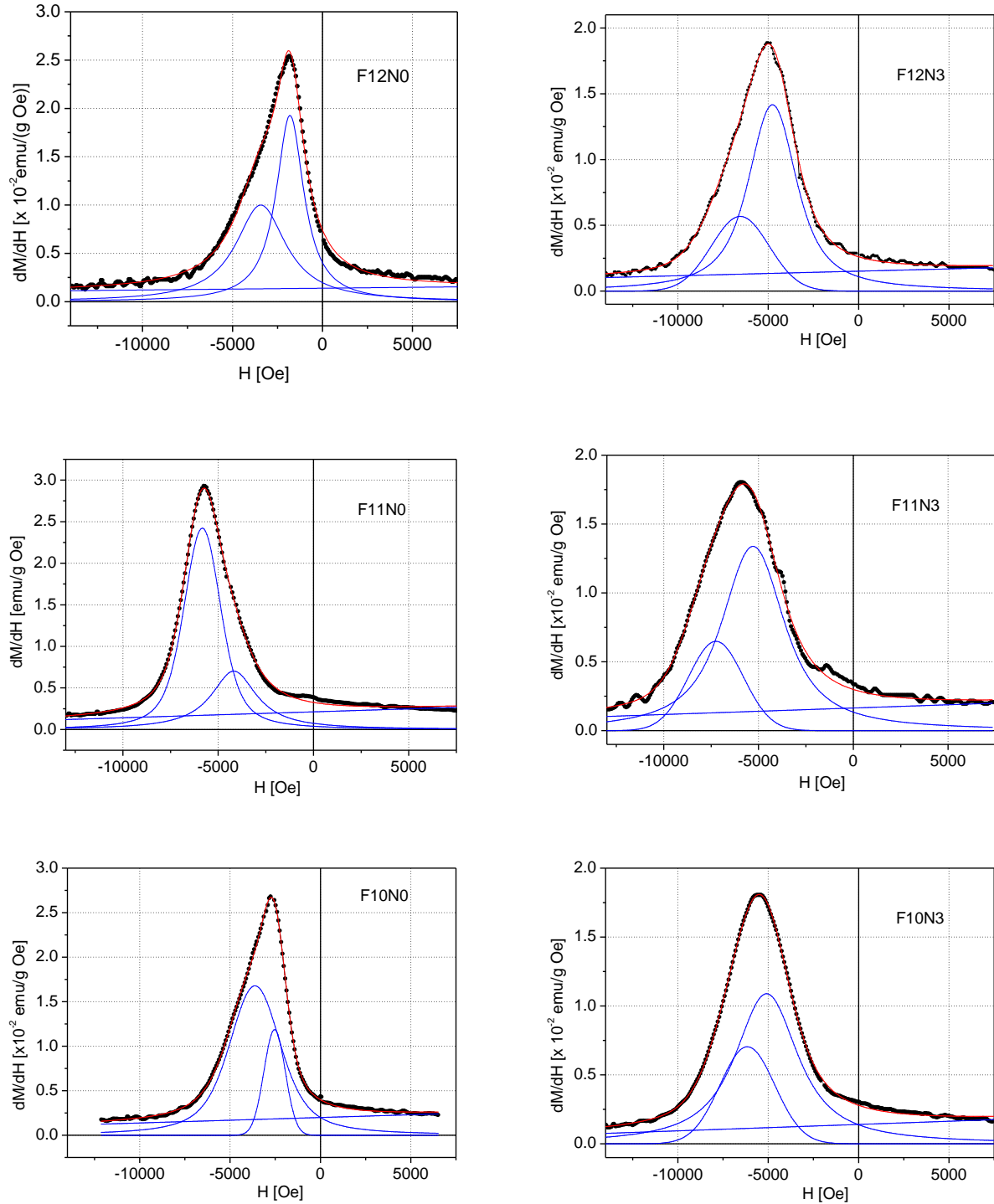
Fig. 8. Magnetic susceptibility χ=d*M*/d*H* (dots) and Voigt fits (lines).

The Curie temperature T_C of sample F11N3 was determined with the aid of thermo-gravimetrical TG measurements under an applied magnetic field. Figure 9 shows the weight *W vs* temperature *T* curve obtained for this sample. Two ferro- to- paramagnetic transitions are noticed as two steps in the TG curve.

The inset of Figure 9 shows the derivative d*W*/d*T* with the two maxima corresponding to the two transitions. T_C was calculated using the tangent method, not as the maxima of *W vs T*. The observation of two Curie temperatures at T_C1 and T_C2 ($>T_C1$) provides additional support of the

presence of two magnetic arrangements, one corresponding to a moderate ordered structure and another to a more anisotropic one. An exhaustive analysis on this effect was reported in a previous paper [18].
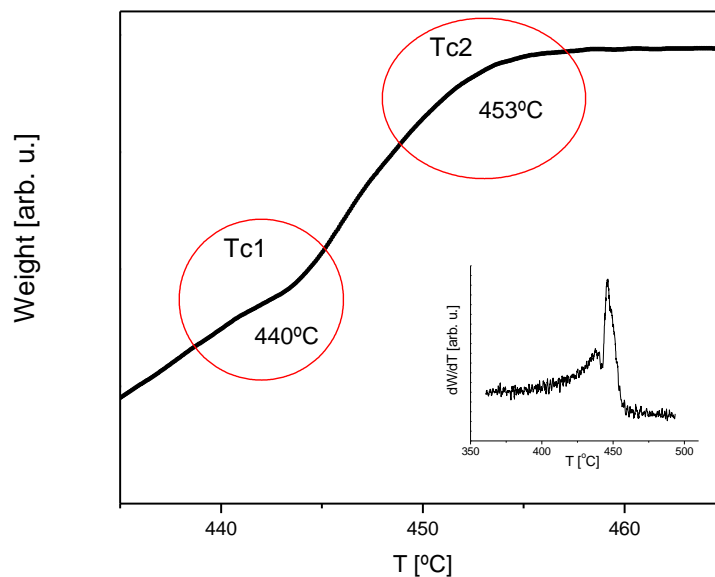
Fig. 9. Weight *vs* temperature obtained for sample F11N3 with an applied magnetic field. Inset: Derivative of the curve, showing two maxima corresponding to two ferro- to- paramagnetic transitions.

4. Summary

Nd-Co substituted hexaferrites with different iron content were successfully prepared by the self combustion method and calcination for short times (2 h) in air, at 1100 ^{o}C. Magnetic properties enhance with substitution in all samples. Substituted samples with a 11:1 Fe/Sr ratio present the best magnetic properties, followed by substituted samples with Fe/Sr ratios of 10 and 12. Iron deficiency in the formulation enhances the magnetic properties of the studied hexaferrites, favoring sites occupancy and obtaining M_r/M_S ratios which are comparable to the stoichimetric formulation. Mössbauer analysis shows that iron occupancy is related to magnetization values and that hyperfine parameters reflect the changes that take place in the hexaferrite structure upon Fe defect and substitution of Fe and Sr by Co and Nd, respectively. There is an optimal iron content in substituted hexaferrite, which is not the stoichiometric value. This value is low enough to admit Nd and Co incorporation in the appropriate sites to result in a more anisotropic structure. The existence of two different magnetic orderings in the structure is found to enhance anisotropy and therefore coercivity.

References
[1]   H. Kojima in: E.P. Wohlfarth (Ed.), Handbook of Ferromagnetic Materials, vol. 3, North-Holland, Amsterdam, 1982, pp. 305−391.

[2]   S.E. Jacobo, L. Civale, M.A. Blesa, Evolution of the magnetic properties during the thermal treatment of barium hexaferrite precursors obtained by coprecipitation from barium ferrate (VI) solutions, J. Magn. Mag. Mat. 260 (2003) 37−41.

[3]   P.G. Bercoff, H.R. Bertorello, Magnetic properties of hematite with large coercivity, Appl. Phys. A 100 (4) (2010) 1019−1027.

[4]   P.G. Bercoff, H.R. Bertorello, Magnetic properties of Ba hexaferrite and Fe compounds produced by milling and annealing in air, J. Magn. Magn. Mater. 205 (1999) 261−269.

[5]   C.R. Lin, Y.J. Siao, M.H. Hsieh, Magnetic properties of lead ferrite nanoparticles prepared by the polymerized complex method, J. All. Comp. 462 (2008) 315.

[6]   R.Q. Guo, M.G. Gu, H.G. Li, W. Huang, P.M. Sun, Y.P. Jin, Effect of precursor solutions with different composition on synthesis of ultrafine $BaLa_{0.3}Fe_{11.7}O_{19}$ using sol-gel auto-combustion technique, J. Mater. Sci. 39 (2004) 987-991.

[7]   Y.P. Fu, C.H. Lin, Fe/Sr ratio effect on magnetic properties of strontium ferrite powders synthesized by microwave-induced combustion process, J. All. Comp. 386 (2005) 222-227.

[8]   M. I. Oliva, P. G. Bercoff, H. R. Bertorello, First order reversal curves analysis of the temperature effect on magnetic interactions in barium ferrite with La-Co addition, Phys. B, 404, 18 (2009) 2742-2745.

[9]   F. Kools, A. Morel, R. Grössinger, J.M. Le Breton, P. Tenaud, LaCo-substituted ferrite magnets, a new class of high-grade ceramic magnets; intrinsic and microstructural aspects, J. Magn. Magn. Mater. 242−245 (2002) 1270−1276.

[10] L. Lechevallier, J.M. Le Breton, A. Morel, P. Tenaud, Influence of the presence of Co on the rare earth solubility in M-type hexaferrite powders, J. Magn. Magn. Mater. 316 (2007) e109−e111.

[11] P. G. Bercoff, C. Herme, S. E. Jacobo, The influence of Nd-Co substitution on non-stoichiometric strontium hexaferrite nanoparticles, J. Magn. Magn. Mater. 321 (2009) 2245-2250.

[12] S. E. Jacobo, C. Herme and P. G. Bercoff, Influence of the iron content on the formation process of substituted Co-Nd strontium hexaferrite prepared by the citrate precursor method, J. All. Comp. 495, 2 (2010) 513–515.

[13] J.F. Wang, C.B. Ponton, I.R. Harris, J. Magn. Magn. Mater. 234 (2001) 233−240.

[14] J. Smit, H.P.J. Wijn, Ferrites, Philips Technical Library, The Netherlands, 1959.

[15] S.E. Jacobo, C. Herme, P.G. Bercoff, Influence of the iron content on the formation process of substituted Co-Nd strontium hexaferrite prepared by the citrate precursor method, J. All. Comp. 495, 2 (2010) 513–515.

[16] N. Rezlescu, C. Doroftei, E. Rezlescu, P.D. Popa, The influence of heat-treatment on microstructure and magnetic properties of rare-earth substituted $SrFe_{12}O_{19}$, J. All. Comp. 451 (2008) 492-496.

[17] R.A. Brand, Normos Programs. Laboratorium fuer Angewandte Physik, Universitaet Duisburg, 1990.

[18] C. Herme, P. G. Bercoff, S. E. Jacobo, Nd-Co substituted strontium hexaferrite powders with enhanced coercivity, Mat. Res. Bull. 47 (2012) 3881-3887.

[19] N. Rezlescu, E. Rezlescu, The influence of Fe substitutions by R ions in a Ni−Zn Ferrite, Sol. St. Comm. 88 (2) (1993) 139-141.

[20] E. Rezlescu, N. Rezlescu, P. Popa, L. Rezlescu, C. Pasnicu, The Influence of R2O3 (R = Yb, Er, Dy, Tb, Gd, Sm and Ce) on the Electric and Mechanical Properties of a Nickel–Zinc Ferrite, Phys. Stat. Sol. A 162 (1997) 673-678.

[21] C. Herme, S. Jacobo, P. G. Bercoff, B. Arcondo, Mössbauer analysis of Nd-Co M-type strontium hexaferrite powders with different iron content, Hyperf. Interact. 195, 1 (2010) 205-212.

[22] Y. Wang, L. Li, H. Liu, H. Qiu, F. Xu, Magnetic properties and microstructure of La-substituted BaCr-ferrite powders, Mat. Letters 62 (2008) 2060–2062.